 CMES, vol.7, no.1, pp.49-67, 2005

A Tangent Stiffness MLPG Method for Atom/Continuum Multiscale Simulation

Shengping Shen[1] **and S. N. Atluri**[1]

Abstract: The main objective of this paper is to develop a multiscale method for the static analysis of a nano-system, based on a combination of molecular mechanics and MLPG methods. The tangent-stiffness formulations are given for this multiscale method, as well as a pure molecular mechanics method. This method is also shown to naturally link the continuum local balance equation with molecular mechanics, directly, based on the stress or force. Numerical results show that this multiscale method quite accurate. The tangent-stiffness MLPG method is very effective and stable in multiscale simulations. This multiscale method dramatically reduces the computational cost, but it still can provide reasonable accuracy in some regions of the model.

keyword: Molecular mechanics, Multiscale method, continuum mechanics, MLPG.

1 Introduction

Recently, an intense effort has been devoted to the modeling and simulations of physical phenomena occurring over a vast range of length scales. This endeavor has prompted the development of multiscale modeling and simulation strategies. *Computational Nanotechnology* [Srivastava and Atluri (2002a, b)] has become an indispensable tool not only in predicting, but also in *engineering* the properties of multi-functional nano-structured materials. The nano-scale is the length scale of individual atoms, i.e. 1-10nm. At such length scales, continuum models are not flexible enough to accommodate the individual atomic scale processes. An alternative to continuum analysis is the atomistic modeling and simulation, in which individual atoms are explicitly followed during their evolution. Even though this atomistic modeling can trace all the details of an atomic-scale processe, it has its own set of limitations. When the length-scale cannot be accessed by either continuum methods because it is too small for averaging, or the atomistic methods because it is too large for simulations on the present day computers, these two approaches become inadequate, and that has presented significant challenges to the scientific community. A recent review of the computational nano-mechanics can be found in Shen and Atluri (2004b).

For phenomena on a much larger space scale, one possible strategy is the multi-scale methods. The simulation of large systems must be left to continuum methods. Continuum mechanics is used to predict the phenomena described by uniform collective behavior of atoms, while nano-mechanics is used to predict the phenomena described by dramatic changes in the state of a few atoms. Multiscale modeling and simulations are being used in diverse fields, such as materials science, nano/microelectronics, environmental remediation, and biotechnology. The overall goal of multiscale modeling is to predict the response of complex systems across all relevant spatial scales. It is of interest to build models that can seamlessly simulate multi-scale systems. Several methods have been developed for the multiscale simulations.

The quasicontinuum method, introduced by Tadmor et al. (1996), and further developed by Chung and Namburu (2003), gives a theory for bridging the atomistic and continuum scales in *quasistatic problems*. In this method, a set of atoms making up a Bravais lattice is selected from a subset. A triangulation of this subset allows the introduction of finite element-like shape functions at lattice points, allowing the interpolation of quantities at intermediate points in the lattice. Thus, the problem of the minimization of energy to find equilibrium configurations can be written in terms of a reduced set of variables. The method is made practical by approximating summations over all atoms, by using summation rules analogous to numerical quadrature. The rules rely on the smoothness of the quantities over the size of the triangulation to ensure accuracy. This method is limited to the case of a zero temperature.

[1] Center for Aerospace Research & Education
University of California at Irvine
5251 California Avenue, #140
Irvine, CA 92617, USA

Another approach to the coupling of the length scales is the FE/MD/TB model of Abraham (2000). In this method, three simulations are run simultaneously, using the finite element method (FEM), molecular dynamics (MD), and semi-empirical tight binding (TB). Each simulation is performed on a different region of the domain, with a coupling imposed in "handshake" regions where the different simulations overlap. The challenge for mesh generation is that the mesh should smoothly transition between the true atomic lattice in the MD region and the closet-packed FE meshes. Too abrupt a crossover leads to unphysical behavior, such as elastic wave resonances at the interface. Wagner and Liu (2003) presented a multiscale method for coupling molecular dynamics and continuum mechanics by using "bridging scale" decomposition and quasicontinuum method [Tadmor et al. (1996)]. We developed a method for the seamlessly coupling of continuum and MD simulation at finite temperature [Shen, and Atluri (2004a)], where alternate interfacial conditions between atomistic and continuum regions were proposed by considering the fluctuation of atoms in the continuum region. Its effectiveness in ensuring the accurate passage of information between atomistic and continuum regions was discussed [Shen, and Atluri (2004a)].

This paper is the extension of Shen and Atluri (2004a), which focused on the finite temperature, dynamic problems. A multiscale method for coupling the continuum models with molecular models at *the 0° temperature are developed here for static problems*, based on the meshless local Petrov-Galerkin (MLPG) method. For the static molecular mechanics, the tangent stiffness formulation is used. A multiscale system is divided in to two regions: an atomistic region, which may contain inhomogeneities, and an equivalent continuum mechanics (ECM) domain, which is defect-free. In the (ECM) region, the deformation is homogeneous, and thus can be approximated by an equivalent continuum mechanics model as in the quasicontinuum method. However, in contrast to quasicontinuum method, there is no "spurious force" to appear near the interface in this method. The material in ECM is discritized into a set of nodes, which are not necessarily coincident with the atoms. The positions of the atoms in this region can be interpolated from those of the nodes. The tangent stiffness MLPG method is employed to solve for the displacements of the nodes in the ECM region.

2 The MLPG Method and Radial Basis functions

Due to their flexibility and potential in negating the need for the human-labor intensive process of constructing geometric meshes, meshless methods, as alternative numerical approaches to eliminate the well-known drawbacks in the finite element and boundary element methods, have attracted much attention in recent decades,.

The MLPG method is a simple and less-costly alternative to the FEM and BEM [Atluri and Zhu (1998), Atluri and Shen (2002a), Atluri (2004)]. The main objective of the meshless methods is to alleviate the difficulty of, meshing and remeshing the entire structure; by only adding or deleting nodes in the entire structure, instead. The meshless local Petrov-Galerkin (MLPG) method is truly meshless, as no finite element/or boundary element meshes are required in this approach, either for purposes of interpolation of the trial and test functions for the solution variables, or for the purpose of integration of the 'energy'. Remarkable successes of the MLPG method have been reported in solving the convection-diffusion problems; fracture mechanics; Navier-Stokes flows; and plate bending problems. Recently, the MLPG method has made some strides, and it is applied successfully in studying strain gradient materials [Tang, Shen and Atluri, (2003)), three dimensional elasticity problems [Li, Shen, Han and Atluri (2003), Han and Atluri (2004a)], and elstodynamics [Han and Atluri (2004b)]. The MLPG method was also extended to solve the boundary integral equations [Atluri, Han and Shen (2003), and Han, Atluri (2003)].

Six different nodal-based local test functions may be selected, which lead to six different MLPG methods. Based on the MLPG concept, these variants of the MLPG method are labeled as MLPG1, MLPG2, MLPG3, MLPG4, MLPG5, and MLPG6, respectively. Among them, MLPG5 does not involve either a domain, or a singular integral, to generate the stiffness matrix; it only involves the regular boundary integral. Thus, it is a highly promising MLPG method while, numerical examples validate that the MLPG5 method is fast, accurate and robust.

In the conventional Galerkin method, the trial and test functions are chosen from the same function-space. In MLPG, the nodal trial and test functions can be different: the nodal trial function may correspond to any one of MLS, PU, Shepard function, or RBF types of inter-

polations; and the test function may be totally different, and may correspond to any one of MLS, PU, Shepard function, RBF, a Heaviside step function, a Dirac delta function, the Gaussian weight function of MLS, a special form of the fundamental solution to the differential equation, or any other convenient function, in the support domain, Ω_{te}, of the test function. Furthermore, the physical sizes of the supports (Ω_{tr} and Ω_{te}, respectively) of the nodal trial and test functions may be different. These features make the MLPG method very flexible. The MLPG method, based on a local formulation, can include all the other meshless methods based on global formulation, as special cases [see Atluri (2004)].

In this paper, we choose the *local* radial basis functions [Hardy (1971), Wendland (1999), Liu and Gu (2001)] to interpolate the trial functions, because of its Kronecker Delta property. Consider a continuous function $u(\mathbf{x})$ defined in a domain Ω, discretized by a set of nodes. An interpolation of $u(\mathbf{x})$ from the neighboring nodes of a point $\mathbf{x}_\alpha$ within the domain Ω, using RBFs and a polynomial basis, can be written as

$$\begin{aligned} u(\mathbf{x}) &= \sum_{i=1}^{n} R_i(\mathbf{x})\, a_i(\mathbf{x}_\alpha) + \sum_{j=1}^{m} p_j(\mathbf{x})\, b_j(\mathbf{x}_\alpha) \\ &= \mathbf{R}^T\mathbf{a} + \mathbf{P}^T\mathbf{b} \end{aligned} \tag{1}$$

where $R_i(\mathbf{x})$ is the radial basis function, $p_j(\mathbf{x})$ is a monomial in the space coordinates, n is the number of nodes in the neighborhood of $\mathbf{x}_\alpha$, m is the number of polynomial basis functions (usually $m \ll n$), and $a_i(\mathbf{x}_\alpha)$ and $b_j(\mathbf{x}_\alpha)$ are the coefficients for $R_i(\mathbf{x})$ and $p_j(\mathbf{x})$, respectively, corresponding to the point $\mathbf{x}_\alpha$. The number of the neighbor nodes of $\mathbf{x}_\alpha$ is not greater than the total number of nodes in the global domain.

The radial basis function has the following general form

$$R_i(\mathbf{x}) = R_i(r_i) \tag{2}$$

where $r_i = \|\mathbf{x} - \mathbf{x}_i\|$. The polynomial term is added to ensure the consistency and the condition of the non-singularity of the RBFs approximation, which should satisfy the following constraints

$$\sum_{i=1}^{n} p_j(\mathbf{x}_i)\, a_i = 0,\ j = 1,2,\cdots,m \tag{3}$$

The coefficients are determined by enforcing the interpolation pass through all n scattered nodes within the influence domain:

$$u(\mathbf{x}_k) = \sum_{i=1}^{n} R_i(\mathbf{x}_k)\, a_i + \sum_{j=1}^{m} p_j(\mathbf{x}_k)\, b_j,\ k = 1,2,\cdots,n \tag{4}$$

Then, the interpolation is expressed as

$$u(\mathbf{x}) = \begin{bmatrix} \mathbf{R}^T(\mathbf{x}) & \mathbf{P}^T(\mathbf{x}) \end{bmatrix} \mathbf{A}^{-1} \begin{Bmatrix} \mathbf{u}_e \\ \mathbf{0} \end{Bmatrix} = \boldsymbol{\phi}(\mathbf{x})\, \mathbf{u}_e \tag{5}$$

where

$$\mathbf{A} = \begin{bmatrix} \mathbf{R}_0 & \mathbf{P}_0 \\ \mathbf{P}_0^T & \mathbf{0} \end{bmatrix} \tag{6}$$

$$\mathbf{R}_0 = \begin{bmatrix} R_1(\mathbf{x}_1) & R_2(\mathbf{x}_1) & \cdots & R_n(\mathbf{x}_1) \\ R_1(\mathbf{x}_2) & R_2(\mathbf{x}_2) & \cdots & R_n(\mathbf{x}_2) \\ \vdots & \vdots & \vdots & \vdots \\ R_1(\mathbf{x}_n) & R_2(\mathbf{x}_n) & \cdots & R_n(\mathbf{x}_n) \end{bmatrix}_{n\times n} \tag{7}$$

$$\mathbf{P}_0 = \begin{bmatrix} p_1(\mathbf{x}_1) & p_2(\mathbf{x}_1) & \cdots & p_m(\mathbf{x}_1) \\ p_1(\mathbf{x}_2) & p_2(\mathbf{x}_2) & \cdots & p_m(\mathbf{x}_2) \\ \vdots & \vdots & \vdots & \vdots \\ p_1(\mathbf{x}_n) & p_2(\mathbf{x}_n) & \cdots & p_m(\mathbf{x}_n) \end{bmatrix}_{n\times m} \tag{8}$$

$$\mathbf{u}_e = [u_1, u_2, \cdots, u_n]^T \tag{9}$$

and the matrix of the shape functions $\phi(\mathbf{x})$ is defined by

$$\boldsymbol{\phi}(\mathbf{x}) = \left[\phi^1(\mathbf{x}), \phi^2(\mathbf{x}), \cdots, \phi^i(\mathbf{x}), \cdots, \phi^n(\mathbf{x})\right] \tag{10}$$

with

$$\phi^k(\mathbf{x}) = \sum_{i=1}^{n} R_i(\mathbf{x})\, \hat{\mathbf{A}}_{ik} + \sum_{j=1}^{m} p_j(\mathbf{x})\, \hat{\mathbf{A}}_{(n+j)k} \tag{11}$$

where $\hat{\mathbf{A}}_{ik}$ represents the (i,k) element of matrix $\mathbf{A}^{-1}$.

The widely used RBFs include multiquadrics (MQ), Gaussian (EXP), and thin plate splines (TPS) forms, and so on. In this paper, we will employ the multiquadrics (MQ) form:

$$R_i(\mathbf{x}) = \left(r_i^2 + c^2\right)^{\beta} \tag{12}$$

c and β are the shape parameters. Here, we choose $c = 1$, $\beta = 1.03$ or $c = 2$, $\beta = 1.99$, that we denote RBF1 and RBF2, respectively, hereafter in this paper.

3 The MLPG Method for Equivalent Continuum

In this section, a finite deformation model based on the atomistic physics will be developed, for use in the ECM region.

In continuum mechanics, the stress at a material point is a function of the 'state' variables, such as strain, and its gradients, at the same point. In order to formulate a constitutive law for an *equivalent continuum model* (ECM) from the atomic forces, a hypothesis to connect the continuum displacement field and the motions of atoms must be employed. The Cauchy-Born hypothesis is the basis for developing the ECM elastic potentials, from the atomistic description of the system. In the absence of slips, phase transitions, twinning or other inelastic phenomena, the Cauchy-Born hypotheses for crystals are equivalent for homogeneous deformations (Ericksen, 1984). Once the geometry of the deformed lattice vectors is linked to the continuum deformation, a constitutive model based on atomistic description can be constructed by equating the continuum strain energy density to the potential energy of the atomic system for a representative cell, divided by its volume, as in Tadmor et al. (1996).

In this paper, first, we will develop an *MLPG tangent-stiffness method for the ECM region*, in which it is assumed that the state of deformation is homogeneous and can be well-characterized by the local deformation gradient **F**. The inhomogeneous deformation, such as near defect cores, will be accounted for by the pure molecular mechanics method. *The whole idea is that: in the ECM, MLPG5 or MLPG1 tangent-stiffness will be employed; in the MD region, the tangent-stiffness molecular mechanics method will be employed.*

Both of these, the ECM and MD regions, are linked through the device of the meshless local Petrov-Galerkin (MLPG) method, which will thus offer the possibility of carrying out uniformly valid simulations of material properties for multi-scale systems at larger length scales than direct atomistic calculations, and permits a reduction of the full set of atomic degrees of freedom; thus reaching towards almost $O(N)$ algorithms. This is illustrated of in Fig. 1. In the ECM region, the nodes can be taken to be arbitrary, and not necessarily be coincident with the atoms. In MD region, the nodes are taken to be the atoms themselves. In the ECM region, the solid points represent the atoms, while the open points represent the nodes of the MLPG method. MLPG5 will be implemented in "ECM" region and molecular mechanics method will be implemented in MD region.

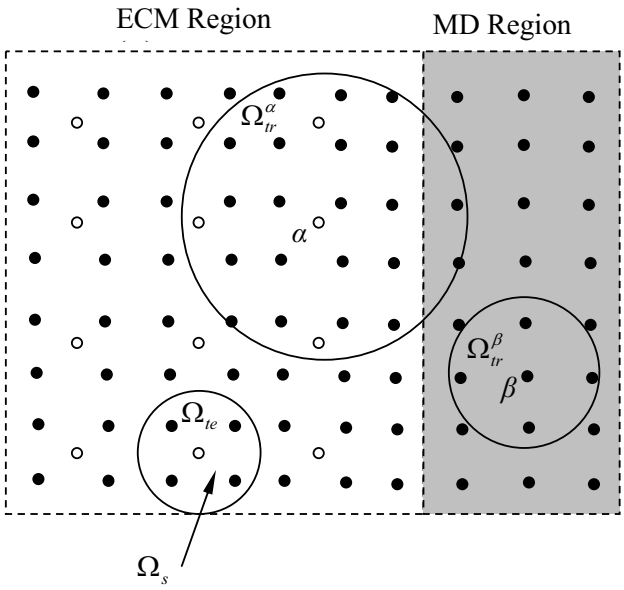

Figure 1 : Illustration of multiscale simulation.

The atomic positions are governed by Newtonian mechanics and described by molecular mechanics. The atomic forces are analytic derivatives of the inter-atomic potential (Born-Oppenheimer expansion). In the ECM, the atomic environment is characterized by the deformation gradient there. *Each continuum point is taken to represent a large region on the atomic scale, which is homogeneously distorted according to the deformation gradient at the point.* The constitutive response in this region is obtained from the atomistic calculation rather than a phenomenological rule, in a way similar to the quasicontinuum method proposed by Tadmor et al. (1996).

By means of the concept of the MLPG, a local weak form (in subdomain Ω_s, as in Fig. 1) for the Newton's law of motion (conservation of linear momentum) will be used to derive a system of equations for multi-scale materials modeling. In this paper, we choose radial basis function to be the interpolation scheme, due to its convenience in this case and their Kroneck Delta property [Atluri (2004), Atluri & Shen (2002a, b)].

In classical continuum mechanics, a point $\mathbf{X}$ in the undeformed body Ω_0 in the reference frame is mapped to a point $\mathbf{x}$ in its current shape Ω in the current frame. The deformed configuration of the body is described by a displacement function $\mathbf{u}(\mathbf{X})$, which represents the displacement at point $\mathbf{X}$, as

$$\mathbf{x} = \mathbf{X} + \mathbf{u}(\mathbf{X})$$

The deformation gradient is defined by

$$\mathbf{F} = \frac{\partial \mathbf{x}}{\partial \mathbf{X}} = \mathbf{I} + \frac{\partial \mathbf{u}}{\partial \mathbf{X}}$$

to map infinitesimal material vector from the undeformed body Ω_0 into the deformed one Ω. Here, $\mathbf{I}$ is the identity tensor.

In the molecular dynamics region, the initial position of an atom I is denoted as $\mathbf{X}_I$. The current configuration of the atom is described by a displacement $\mathbf{u}$ which depends on $\mathbf{X}$, and can be written as

$$\mathbf{x}_I = \mathbf{X}_I + \mathbf{u}_I \tag{13}$$

where $\mathbf{u}_I$=$\mathbf{u}(\mathbf{X}_I)$.

The distance between two atoms I and J in the reference configuration can be written as

$$\mathbf{R}_{IJ} = \mathbf{X}_J - \mathbf{X}_I \tag{14}$$

The distance between two atoms I and J in the current configuration can be written as

$$\mathbf{r}_{IJ} = \mathbf{x}_J - \mathbf{x}_I \tag{15}$$

According to the Cauchy-Born rule (Ericksen, 1984), for simple Bravais lattice that has the centrosymmetric atomic structure, we have

$$\mathbf{r}_{IJ} = \mathbf{F}\mathbf{R}_{IJ} \tag{16}$$

However, it does not hold for a ccomplex Bravais lattice which can be given by means of a number of interpenetrating simple Bravais lattices (sub-lattices), and in case which do not possess centrosymmetry, such as the hexagonal lattice. In this case, the Cauchy-Born rule gives [Zanzotto (1996), Martin (1975), Cousins (1978), Born and Huang (1954)]

$$\mathbf{r}_{IJ} = \mathbf{F}\mathbf{R}_{IJ} + \varsigma_k \tag{17}$$

where the internal variable ς_k are shift vectors, with k ranging from 0 to some integer N (There are N+1 sublattices in the complex Bravais lattice. If atoms I, J are in the same sub-lattices, $\varsigma_k = 0$). ς_k and $\mathbf{F}$ are the independent variables. At the static equilibrium state, the vectors ς_k are to be determined by the minimization of the energy function, so as to reach an equilibrium configuration in the deformed crystal. This means that the equilibrium values of ς_k can be written as functions of $\mathbf{F}$.

It is noted that, in order to apply the Cauchy-Born rule to nanotubes or fullerenes, a more general exponential mapping procedure like the one in Arroyo and Belytchko (2002) should be used. Since nanotube is only a few atom-thick, the continuum measures, such as stress and strain, lose their meanings in such a situation. An alternative multiscale method for a nanotube, which abandons the Cauchy-Born rule, as discussed in Shen and Atluri (2004c), will be shown in an upcoming paper.

The right Cauchy-Green strain tensor is defined by

$$\mathbf{C} = \mathbf{F}^T\mathbf{F} \tag{18}$$

and the Green strain tensor is defined by

$$\mathbf{E} = \frac{1}{2}(\mathbf{C} - \mathbf{I}) \tag{19}$$

The kinematics of the deformation is characterized by the deformation gradient. The constitutive nature of the material is obtained through the strain energy density function W which relates the energy at a point to the local

state of deformation there. It may be shown that W can only be a function of $\mathbf{F}$, from the hypothesis of locality and use the entropy production inequality. Moreover, according to the postulate of material frame indifference, it can be shown that the dependence of W on $\mathbf{F}$ can only be through the right Cauchy-Green tensor $\mathbf{C}$. However, in this paper, for convenience, we will employ the deformation gradient $\mathbf{F}$ as the strain.

Following the classical continuum mechanics, the first Piola-Kirchhoff stress $\mathbf{T}$ can be defined as

$$\mathbf{T} = \frac{\partial W}{\partial \mathbf{F}} \tag{20}$$

The conservation of linear momentum leads to:

$$\nabla \cdot \mathbf{T} + \mathbf{f} = 0 \tag{21}$$

where $\nabla\cdot$ denotes the divergence taken with respect to the material frame, $\mathbf{f}$ is the body force.

The conservation of angular momentum leads to:

$$\mathbf{FT} = (\mathbf{FT})^T \tag{22}$$

The tangent stiffness material-moduli (Lagrangian elasticity tensor) can be defined as

$$\mathbf{D} = \frac{\partial^2 W}{\partial \mathbf{F} \partial \mathbf{F}} \tag{23}$$

More details about the finite strain analysis can be found in Atluri (1979, 1980).

The *local weak form* of equation (21) can be written as

$$\int_{\Omega_s} (\nabla \cdot \mathbf{T} + \mathbf{f}) \mathbf{V} d\Omega = 0 \tag{24}$$

where $\mathbf{V}$ is the test function in the local domain Ω_s in the reference frame. The local symmetric weak form can be written as

$$\begin{aligned} &-\int_{\Omega_s} T_{Kl} V_{l,K} d\Omega + \int_{L_s} T_{Kl} n_K V_l d\Gamma \\ &+ \int_{\Gamma_{su}} T_{Kl} n_K V_l d\Gamma = -\int_{\Gamma_{st}} T_{Kl} n_K V_l d\Gamma \end{aligned} \tag{25}$$

where $\mathbf{n}$ is the unite normal to the local boundary surface Γ_s of Ω_s. The corresponding MLPG5 weak-form (when the test functions are taken to Heaviside functions) is:

$$\int_{L_s} T_{Kl} n_K d\Gamma + \int_{\Gamma_{su}} T_{Kl} n_K d\Gamma = \int_{\Gamma_{st}} T_{Kl} n_K d\Gamma \tag{26}$$

Actually, the *MLPG5 [equation (26)] can be directly derived from the conservation of linear momentum in an arbitrary local domain, which is the basis of the finite deformation theory.* The physical basis of the MLPG5 is the conservation of linear momentum in an arbitrary local domain, and that of the MLPG2 is the conservation of linear momentum on arbitrary point.

A corresponding continuous interpolation will replace the piece-wise function for the position of the atom in the ECM region,

$$\mathbf{x} = \sum_{\alpha=1}^{N} \phi^{\alpha}(\mathbf{X}) \mathbf{x}_{\alpha} \tag{27}$$

$\mathbf{x}_{\alpha}, \alpha = 1, 2, \ldots, N$, in equation (27), are the nodal values. $\phi^{\alpha}(\mathbf{X})$ is the RBF shape function.

Assume that there are N_1 atoms in molecular mechanics region (MM), and N_2 in ECM region (ECM). The displacements of atoms I in the MM region are denoted by $\mathbf{q}_I$ $(1 \le I \le N_1)$. The displacements of *atom i* in the ECM region are denoted by $\mathbf{u}_i$ $(1 \le i \le N_2)$, which are interpolated from the displacements of the *nodes* in ECM region, as

$$\mathbf{u}_i = \mathbf{u}(\mathbf{X}_i) = \sum_{\alpha=1}^{N} \phi^{\alpha}(\mathbf{X}_i) \mathbf{u}_{\alpha} \tag{28}$$

Here, $\mathbf{u}_{\alpha}$, α=1, 2,..., N, are the nodal values. It is noted that N is less than the amount of atoms of ECM region, i.e., $N \le N_2$, and the node is not necessarily an atom. The displacement $\mathbf{u}_i$ of an atom in ECM region implies an average value of the atomic displacement, and can not catch the thermal fluctuations.

4 The Atomistic Constitutive Law in ECM and MLPG5

In classical MD, each atom moves and acts simply as a particle that is moving in a many-body force field of

other similar particles. The atomic and molecular interactions describing the dynamics are given by classical many-body force-field functions, and the interatomic potential Π as an infinite sum over pair, triplet, etc.. The potential of the atoms is calculated by building the appropriate complement of neighbors in the molecular mechanics region. As is well known, it is computationally expensive to calculate the interatomic potential and the atomic force, since we should visit each atom.

In this paper, an important procedure is to estimate the strain energy density in the ECM If we sum over all the atoms as in the classical molecular dynamics, we can certainly get the energy density by evaluating Π/Ω. However, this is very expensive. In the quasicontinuum method [Tadmor et al. (1996)], for a homogeneously distorted crystal, the continuum strain energy density is obtained by equating to the potential energy of the atomic system for a representative cell divided by its volume, which means that the calculation of the interatomic potential and the atomic force is limited *to a single unit cell*. In the ECM regions, the energy is calculated using a single representative cell in the center of a uniformly deformed crystal. This crystal is always made sufficiently large or periodic that there are no boundary effects there either. In practice, the calculation of the energy is performed separately from the real model in a *virtual* representative cell. Suppose there is a point (for example, the Gaussian point in the local domain) where the deformation gradient is $\mathbf{F}$. Then we take a large crystallite of the material (periodic or infinite structure) and apply the deformation gradient $\mathbf{F}$ to the crystallite, i.e., we move the atoms of a single representative cell to the positions given by the deformation gradient. Now, based on this, we can calculate the energy of the single representative cell in this large crystallite, stress tensor, and elasticity tensor, etc.. In this treatment, we do not need consider the real atomic structure of the model, neither need visit every atom. The energy only depends on the gradient $\mathbf{F}$. The energy density on a point (Gaussian point) is then given by

$$W = \frac{\Pi_r}{\Omega_r} - \frac{\Pi_{r0}}{\Omega_r} \tag{29}$$

where Ω_r is the volume of the single representative cell (in the undeformed configuration), Π_{r0} is the potential energy in the unstrained state, and Π_r is the potential energy of the representative cell when its atomic position moved according to $\mathbf{F}$. It is noted that both the interatomic potential energy and the strain energy, involve reference states. The former is referenced to infinitely separated atoms, and the latter is referenced to the unstrained configuration. Hence, the constant offset energy Π_{r0}, representing the potential energy in the unstrained state, which does not affect the dynamics is subtracted in equation (29). However, the energy of a point near a free surface is not computed correctly - this is one of the approximations inherent to the method. After obtaining the strain energy density by the Cauchy-Born rule for certain gradient $\mathbf{F}$, the corresponding first Piola-Kirchhoff stress $\mathbf{T}$, and the tangent stiffness moduli $\mathbf{D}$, in the ECM can be obtained from equations (20) and (23), respectively. In Chung, Namburu, and Henz (2004), the calculation of the energy of each element still needs to visit each atom.

The equations from the nonlinear local Petrov-Galerkin formulation (25), can be solved by employing Newton-Raphson method. Assuming that the equation (25) is at iteration step n, then from step n to step (n+1), the incremental constitutive relation in the ECM can be expressed as

$$\Delta\mathbf{T} = \mathbf{D}{:}\Delta\mathbf{F} = \mathbf{D}{:}\nabla\Delta\mathbf{u} \tag{30}$$

or

$$\Delta T_{Kl} = D_{KlmN}\Delta u_{m,N} \tag{31}$$

where $\Delta\mathbf{u}$ is the increment of the displacement, i.e.,

$$\Delta\mathbf{u} = {}^{n+1}\mathbf{u} - {}^{n}\mathbf{u} \tag{32}$$

with ${}^{n}\mathbf{u}$ denotes the displacement $\mathbf{u}$ at iteration step n. Equation (25) at iteration step (n+1) can be linearized as

$$-\int_{\Omega_s} \Delta T_{Kl} V_{l,K} d\Omega + \int_{L_s} \Delta T_{Kl} n_K V_l d\Gamma + \int_{\Gamma_{su}} \Delta T_{Kl} n_K V_l d\Gamma = Q \tag{33}$$

and

$$Q = -\int_{\Gamma_{st}} T_{Kl} n_K V_l d\Gamma - \int_{\Omega_s} f_l V_l d\Omega$$
$$-\int_{\Gamma_{st}} \Delta T_{Kl} n_K V_l d\Gamma - \int_{\Omega_s} \Delta f_l V_l d\Omega$$
$$+\int_{\Omega_s} T_{Kl} V_{l,K} d\Omega - \int_{L_s} T_{Kl} n_K V_l d\Gamma$$
$$-\int_{\Gamma_{su}} T_{Kl} n_K V_l d\Gamma \tag{34}$$

If we adopt the MLPG5 method, equation (33) and (34) can be rewritten as

$$\int_{L_s} \Delta T_{Kl} n_K d\Gamma + \int_{\Gamma_{su}} \Delta T_{Kl} n_K d\Gamma = Q_l \tag{35}$$

and

$$Q_l = -\int_{\Gamma_{st}} T_{Kl} n_K d\Gamma - \int_{\Omega_s} f_l d\Omega$$
$$-\int_{\Gamma_{st}} \Delta T_{Kl} n_K d\Gamma - \int_{\Omega_s} \Delta f_l d\Omega$$
$$-\int_{L_s} T_{Kl} n_K d\Gamma - \int_{\Gamma_{su}} T_{Kl} n_K d\Gamma \tag{36}$$

By using the natural boundary on Γ_t, $T_{Kl} n_K = \overline{P}_l$, equation (36) can be written as

$$Q_l = -\int_{\Gamma_{st}} \overline{P}_l d\Gamma - \int_{\Omega_s} f_l d\Omega$$
$$-\int_{\Gamma_{st}} \Delta \overline{P}_l d\Gamma - \int_{\Omega_s} \Delta f_l d\Omega$$
$$-\int_{L_s} T_{Kl} n_K d\Gamma - \int_{\Gamma_{su}} T_{Kl} n_K d\Gamma \tag{37}$$

According to equation (4.2), equation (33) or (35) is a linear equation in terms of $\Delta\mathbf{u}$. The increment of displacement, $\Delta\mathbf{u}$, can be interpolated in the MLPG method as

$$\Delta\mathbf{u} = \sum_{\alpha=1}^{N} \phi^{\alpha}(\mathbf{X}) \Delta\mathbf{u}_{\alpha} \tag{38}$$

$\Delta\mathbf{u}_{\alpha}, \alpha = 1, 2, \ldots, N$, in equation (38), are the nodal values. Again, it is noted that N is less than the amount of atoms of the system, and the node is not necessarily the atom. For convenience, we rewrite equation (38) as

$$\Delta u_I = \sum_{\alpha=1}^{N} \phi_{IJ}^{\alpha}(\mathbf{X}) \Delta u_{\alpha J} \tag{39}$$

with $\phi_{IJ}^{\alpha} = \phi^{\alpha} \delta_{IJ}$.

Substitution of equation (39) into equation (35), for all nodes, leads to the following discretized system of linear equations:

$$\sum_{\beta=1}^{N} \left[{}^{n}\mathbf{K}_{\alpha\beta} \Delta\mathbf{u}_{\beta} \right] = {}^{n}\mathbf{Q}_{\alpha} \tag{40}$$

where ${}^{n}\mathbf{K}_{\alpha\beta}$ is defined as the tangent stiffness at step n,

$$\left[{}^{n}\mathbf{K}_{\alpha\beta} \right]_{lJ} = \int_{L_s} D_{KlmN} n_K \phi_{mJ,N}^{\beta} d\Gamma$$
$$+\int_{\Gamma_{su}} D_{KlmN} n_K \phi_{mJ,N}^{\beta} d\Gamma \tag{41}$$

$$\left\{ {}^{n}\mathbf{Q}_{\alpha} \right\}_l = \int_{\Gamma_{st}} \overline{P}_l d\Gamma + \int_{\Omega_s} f_l d\Omega + \int_{\Gamma_{st}} \Delta\overline{P}_l d\Gamma$$
$$+\int_{\Omega_s} \Delta f_l d\Omega - \int_{L_s} T_{Kl} n_K d\Gamma - \int_{\Gamma_{su}} T_{Kl} n_K d\Gamma \tag{42}$$

The integration in equations (41) and (42) can employ the Gaussian quadrature. At each Gaussian point, the deformation gradient $\mathbf{F}$ can be obtained by deriving the interpolation with respect to $\mathbf{X}$, then, by deforming the representative cell according to the deformation gradient $\mathbf{F}$, the stress and tangent stiffness tensors can be obtained readily, as described previously. It is shown that no domain integration in involved in equation (3.35), which is an important advantage of MLPG5. In the Newton-Raphson method, the displacement at each iteration are updated by

$${}^{n+1}\mathbf{u} = {}^{n}\mathbf{u} + \Delta\mathbf{u}$$

The procedure continues until $\| {}^{n}\mathbf{Q}_{\alpha} \|$ (or $\|\Delta\mathbf{u}\|$) is reduced sufficiently for all nodes.

It is noted that in ECM region, atoms implicitly contribute to the problem only through the material property tensor.

5 Tangent Stiffness Formulation for Molecular Mechanics

In the inhomogeneous-deformation region, we will employ pure molecular mechanics method. Assume that there are N_1 atoms in this region (MD). The displacement of atom I in this region is denoted as $\mathbf{q}_I$ $(1 \leq I \leq N_1)$. Now, the control equation will be

$$\mathbf{f}_I = 0 \tag{43}$$

$$\mathbf{f}_I = -\frac{\partial \Pi}{\partial \mathbf{x}_I} = -\frac{\partial \Pi}{\partial \mathbf{q}_I} \tag{44}$$

The force $\mathbf{f}_I$ is computed, as it would be in a standard atomistic calculation. In molecular calculation, the evaluation of the interatomic potential energy, and forces, is performed by taking advantage of the neighbor-list of atoms, so that the time for the computation scales with the number of atoms in region A, i.e. it is of order-N_1.

Similar to that in section 3, we can also linearize equation (43) by employing Newton-Raphson method, which was described in Shen and Atluri (2004) for the classical molecular dynamics. Here, we still list these equations for the molecular mechanics. Equation (43) at iteration step (n+1) can be rewritten as

$${}^{n+1}\mathbf{f}_I = 0 \tag{45}$$

Then, equation (45) is written as

$${}^{n+1}\mathbf{f}_I \approx {}^{n}\mathbf{f}_I + \sum_{J=1}^{n} \left(\frac{\partial \mathbf{f}_I}{\partial \mathbf{q}_J} \right) \Delta \mathbf{q}_J = 0 \tag{46}$$

where $\Delta\mathbf{q}$ is the increment of the displacement, i.e.,

$$\Delta \mathbf{q} = {}^{n+1}\mathbf{q} - {}^{n}\mathbf{q} \tag{47}$$

with ${}^{n}\mathbf{q}$ denotes the displacement $\mathbf{q}$ at iteration step n. The above equation can be rewritten as

$$\sum_{J=1}^{N} [{}^{n}\mathbf{K}_{IJ} \Delta \mathbf{q}_J] = {}^{n}\mathbf{Q}_I \tag{48}$$

where the molecular tangent stiffness matrix ${}^{n}\mathbf{K}_{IJ}$ at iteration step n is defined as

$${}^{n}\mathbf{K}_{IJ} = \frac{\partial \mathbf{f}_I}{\partial \mathbf{q}_J} \tag{49}$$

and

$${}^{n}\mathbf{Q}_I = -{}^{n}\mathbf{f}_I \tag{50}$$

The displacement are iteratively updated by

$${}^{n+1}\mathbf{q} = {}^{n}\mathbf{q} + \Delta \mathbf{q} \tag{51}$$

The procedure continues until $\|{}^{n}\mathbf{Q}_\alpha\|$ (or $\|\Delta\mathbf{q}\|$) is reduced sufficiently for all atoms. It is noted that the neighbor list should be renewed every several iteration steps. Now, a unified formulation for the multiscale system can be developed, based on the MLPG method, and the tangent stiffness concept. The equation (40) and (48) can be merged as

$${}^{n}\mathbf{K} \Delta \mathbf{u} = {}^{n}\mathbf{Q} \tag{52}$$

The continuum MLPG5 and molecular mechanics share a common ground of Newton's second law, in the subdomains of each node and to the atoms, respectively. The positions of all nodes in the ECM region are determined by seeking a configuration for which the force in the subdomain of each node is zero. This is similar to the molecular mechanics calculations of atom position, which is based on seeking a configuration for which the force on each atom is zero.

This method should be very effective due to the fact that adaptive remeshing, which is an important factor in multiscale dynamics, is very convenient in the MLPG method. This computational methodology provides a unified method for simulation in MD and equivalent continuum mechanics regions.

6 Interfacial Conditions between Atom and ECM Regions

In the multiscale simulation, the atomistic method is employed where the displacement field varies on an atomic

scale, and the continuum approach is employed elsewhere. Then, the problem is how to link these tow scales together? In dynamic cases, for the seamless multiscale simulation, it is important to ensure that the elastic waves generated in the atomistic region can propagate into the continuum region. Since the continuum region cannot support modes of short wavelength, which is less than the spacing of the nodes, the short waves are reflected back unphysically from an artificial interface or boundary, which may also produce uneven heating across the interface. In order to minimize such reflections, some interfacial conditions are proposed [Cai et al. (2000), E and Huang (2001), Wagner and Liu (2003), Shen and Atluri (2004a)].

As mentioned before, the displacement $\mathbf{u}_i$ of an atom in region B implies an average value of the atomic displacement. As in Shen and Atluri (2004a), to describe it more accurately, we assume that the "real" displacement $\mathbf{q}_i$ of the atom in the region B can be expressed as:

$$\mathbf{q}_i = \mathbf{u}_i + \delta\mathbf{u}_i \tag{53}$$

where $\delta\mathbf{u}_i$ denotes the difference between the atomic displacement and the continuum displacement, and it is assumed that $\delta\mathbf{u}_i << \mathbf{u}_i$ in region B. Now, the total potential energy of the system (A+B) can be written as:

$$\begin{aligned}\Pi(\mathbf{q}_1,\cdots,\mathbf{q}_{N_1+N_2}) &\approx \Pi(\mathbf{u}_i;\mathbf{q}_I) + \sum_{i=1}^{N_2} \frac{\partial\Pi}{\partial\mathbf{q}_i}\Big|_{\mathbf{q}_i=\mathbf{u}_i} \delta\mathbf{u}_i \\ &= \Pi_0 + \sum_{i=1}^{N_2} \frac{\partial\Pi_0}{\partial\mathbf{u}_i}\delta\mathbf{u}_i = \Pi_0(\mathbf{u}_B;\mathbf{q}_A) + \frac{\partial\Pi_0}{\partial\mathbf{u}_B}\cdot\delta\mathbf{u}_B\end{aligned} \tag{54}$$

($I = 1,\cdots,N_1$ in A; $i = 1,\cdots,N_2$ in B)

Here Π_0 denotes the zeroth-order approximation of the potential energy; $\mathbf{q}_A$ and $\mathbf{u}_B$ are the atomic displacement vectors with dimensions $3N_1$ (for 3 dimensions) in region A, and $3N_2$ in region B, respectively; $\delta\mathbf{u}_B$ is a vector with dimension $3N_2$. Effectively, the MLPG algorithm involves an average over the atomic degrees of freedom that are missing from the nodes in region B. The second term in right side of equation (54) accounts for the missing degrees of atomic freedom.

In many of the existing multiscale modeling methods, only the continuum displacements of the atoms, near the interface in the region B, are considered. In this case, in region A, the Newton's Second law can be written in a matrix form as

$$\mathbf{f}_A^0 = -\partial\Pi_0/\partial\mathbf{q}_A = 0 \tag{55}$$

where the force vector $\mathbf{f}_A^0$ is of dimension $3N_1$. Equation (55) will be solved by using the Newton-Raphson method, as discussed in Section 4. Here, the atoms in region B near the atom/ECM interface, we denote them "continuum atom", are needed to calculate the atomic forces in equation (55). The position of these atoms is not calculated from the molecular mechanics (55), but interpolated by the continuum MLPG solution. On the interface of region A and B, the nodes of the ECM region are chosen from the atoms, however, these nodes are only for the interpolation, their position is calculated from the molecular mechanics. Thus, the atomistic governing equations (48) couple the ECM governing equation (40) through the "continuum atom", and the ECM governing equation (40) couple the atomistic governing equations (48) through the interfacial nodes. The degrees of freedom (DOF) N_1 in A are in general greater than these in B, viz., N_2 [i.e., $N_1 >> N_2$]. Thus, this case is computationally inexpensive. The increment of the displacement of "continuum atom" i can be obtained by interpolation as

$$\Delta\mathbf{q}_i = \sum_{\alpha=1}^{N} \phi^\alpha(\mathbf{X}_i)\,\Delta\mathbf{u}_\alpha \tag{56}$$

In this case, the equation (48) is modified to

$$\sum_{J=1}^{N_1} [{}^n\mathbf{K}_{IJ}\Delta\mathbf{q}_J] + \sum_{j=1}^{N_2} {}^n\mathbf{K}_{Ij} \sum_{\alpha=1}^{N} [\phi^\alpha(\mathbf{X}_j)\,\Delta\mathbf{u}_\alpha] = {}^n\mathbf{Q}_I \tag{57}$$

($I,J = 1,\cdots,N_1$ in A; $j = 1,\cdots,N_2$ in B)

However, if we only consider the continuum displacement of the continuum atoms, it will obviously contribute errors to the solution. To improve the performance, Shen and Atluri (2004a) used the first-order approximation of the potential energy, i.e. Π in equation (54), to replace Π_0 in equation (55), which leads to:

$$\mathbf{f}_A^0 - \mathbf{K}_{AB}\delta\mathbf{u}_B = 0 \tag{58}$$

where

$$\mathbf{K}_{AB} = \partial^2\Pi_0/\partial\mathbf{u}_B\partial\mathbf{q}_A.$$

It is noted that the tangent stiffness matrix $\mathbf{K}_{AB}$ is of order $3N_1 \times 3N_2$, and its entries are nonzero only for atomic pairs in the cutoff of the interface. $\delta\mathbf{u}_B$ can be obtained from the equation of atomistic balance in region B, viz.,

$$\mathbf{f}_B = \mathbf{f}_B^0 - \mathbf{K}_{BB}\delta\mathbf{u}_B = 0 \tag{59}$$

with the$3N_2 \times 3N_2$ tangent stiffness matrix

$$\mathbf{K}_{BB} = \partial^2\Pi_0/\partial\mathbf{u}_B\partial\mathbf{u}_B$$

and $\mathbf{f}_B^0$ of dimension $3N_2$ is approximated as

$$\mathbf{f}_B^0 = -\partial\Pi_0/\partial\mathbf{u}_B \tag{60}$$

Thus, by combining equations (58) and (59), we can get the governing equations for the atomic region A:

$$\mathbf{f}_A^0 - \mathbf{K}_{AB}\mathbf{K}_{BB}^{-1}\mathbf{f}_B^0 = 0 \tag{61}$$

Comparing equation (55) with (61), it can be found that the term $-\mathbf{K}_{AB}\mathbf{K}_{BB}^{-1}\mathbf{f}_B^0$ is missing in equation (55), which contributes the errors to the solution. In fact, although the interfacial conditions are very important for dynamic problems (to diminish the reflection of the short wave from the interface) as discussed in Shen and Atluri (2004a), it is unnecessary for static problems. For static problem, the errors can be controlled by properly adjusting the interface where the atom/ECM regions are assembled, or the size of the atomic region. Therefore, in this paper, we just consider equation (55), the effect of the dimension of the atomic region on the accuracy of the solution will be discussed in numerical examples.

The quasicontinuum method [Tadmor et al. (1996)] is based on a well-defined energy functional for the entire system, which lead to spurious forces near the interface, the equilibrium of the system is derived by minimizing the energy functional. These forces arise due to the fact that there is an inherent mismatch between the continuum and atomistic regions in the problem, where different theory is employed to sum the energy in the continuum and atomistic regions, which leads the force on each atom is inconsistent with its status. *The multiscale method developed in this paper is directly based on the stress (ECM) and force (atom), the equilibrium of the system is derived by seeking a configuration for which the force on each degree of freedom is zero. In this method, there are no spurious forces to appear near interface between atomistic and ECM regions*: forces on atoms in the atomistic region near the atom/ECM interface are the same as those of other atoms in the atomistic region, and the stresses of a point in the ECM region near the atom/ECM interface are the same as those of other points in the ECM region.

In general, the combined equations from the nonlinear local Petrov-Galerkin formulation (26), and the atomistic governing equation (43) are solved simultaneously by employing an incremental algorithm. At each incremental load step, a standard Newton-Raphson procedure, as described in Section 4 and 5 for MLPG and molecular mechanics respectively, is used. The total Lagrangean method (T. L.) is employed in this paper.

7 Numerical Examples

This multiscale method can be generalized to multiaxial problems. In this subsection, a planar problem is considered to demonstrate the method without loss of generality. The formulations can be extended to more complicated 3-D systems. The problem is of a graphene sheet of one-atom thickness.

In this example, the Tersoff-Brenner potential [Tersoff (1988), Brenner (1990)] is used for the energy associated with the deformation of the atoms. It is given as a sum over bonds as

$$\Pi = \sum_I \sum_{J(>I)} \left[V_R(r_{IJ}) - \overline{B}V_A(r_{IJ})\right] \tag{62}$$

which has repulsive and attractive terms, respectively,

$$V_R(r_{IJ}) = \frac{f_{IJ}(r)D^{(e)}}{(S-1)}e^{-\sqrt{2S}\beta\left(r-R^{(e)}\right)} \tag{63}$$

$$V_A(r_{IJ}) = \frac{f_{IJ}(r) D^{(e)} S}{(S-1)} e^{-\sqrt{\frac{2}{S}}\beta\left(r-R^{(e)}\right)} \tag{64}$$

with the functions of the bond angle

$$\overline{B} = \frac{1}{2}\left(B_{IJ} + B_{JI}\right) \tag{65}$$

$$B_{IJ} = \left[1 + \sum_{K(\neq I,J)} G(\theta_{IJK}) f_{IK}(r_{IK})\right]^{-\delta} \tag{66}$$

$$G(\theta) = a_0 \left\{1 + \frac{c_0^2}{d_0^2} - \frac{c_0^2}{d_0^2 + (1+\cos\theta)^2}\right\} \tag{67}$$

and the cut-off function which limits the rang of the interactions

$$f_{IJ}(r) = \begin{cases} 1, \; r < R^{(1)} \\ \frac{1}{2} + \frac{1}{2}\cos\left[\frac{\pi\left(r-R^{(1)}\right)}{\left(R^{(2)}-R^{(1)}\right)}\right], \; R^{(1)} < r < R^{(2)} \\ 0, \; r > R^{(2)} \end{cases} \tag{68}$$

where the constants for carbon are

$R^{(e)} = 1.39\text{Å}, \quad D^{(e)} = 6.0 \text{ eV}, \quad S = 1.22,$
$\beta = 2.1\text{Å}^{-1}, \quad \delta = 0.5, R^{(1)} = 1.7\text{Å}, \quad R^{(2)} = 2.0\text{Å},$
$a_0 = 2.0813 \times 10^{-4}, \quad c_0 = 330, \quad d_0 = 3.5$

and 1 ev $= 1.602 \times 10^{-19}$ J.

7.1 The full ECM method

To validate the ECM method, the same examples in Chung, Namburu, and Henz (2004) are calculated in this subsection. The example is that of a 2D graphene sheet of one-atom thickness, the thickness of the sheet is taken to be 3.4 Å, which is the standard layer separation thickness for graphite. At the equilibrium sate, which is taken to be the reference frame, the nearest neighbor bond length is b=1.4507 Å. The displacement is prescribed on the right edge of the graphite sheet, and the left edge is constrained in the X_1-direction and is free in the X_2-direction. As shown in Fig. 2, two loading cases are considered along the right edge of the sheet: a uniform (Case I) and non-uniform (Case II) displacement loading. Case II starts at zero at the top end and linearly increasing to the bottom end. Two sheets are considered: one has 66 atoms with dimensions 1.25632 Å×11.6054 Å, another has 1952 atoms with dimensions 75.3794 Å×68.1819Å.

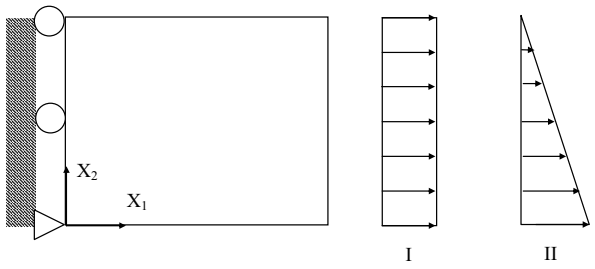

Figure 2 : Graphene under displacement load. Case I is a uniform displacement loading and case II is non-uniform displacement loading.

All the displacement loads are applied in increments. Newton-Raphson iteration is performed in each load increment until nodal displacement increments between iterative steps satisfy $\|\Delta\mathbf{u}\| = \sqrt{\Delta\mathbf{u}\cdot\Delta\mathbf{u}} \leq 10^{-10}$Å. The numerical results are compared with the corresponding results from quenched molecular dynamics in Chung, Namburu, and Henz (2004). We also consider the convergence of this method by using varying node refinements. For the 66-atom sheet, we use 4×4, 6×6, and 10×10 nodes. For the 1952-atom sheet, we use 8×8, 10×10, and 15×15 nodes. The nodes are distributed evenly. In these calculations, the RBF2 is used. For 4×4 and 6×6 nodes, the radius of the trial function domain is taken to be 1.8h, where h represents the distance between the nodes. For 8×8, 10×10, and 15×15 nodes, the radius of the trial function domain is taken to be 3.2h. For all these node refinements, the radius of the test domain is kept to be 0.83h.

Fig. 3 shows the strain energies for 66-atom sheet under uniform displacement load. The results from the quenched MD [Chung, Namburu, and Henz (2004)] are also plotted in this figure, for comparison. The same conclusions as in Chung, Namburu, and Henz (2004) can be reached: the results from this method agree with the results from the quenched MD very well at small strains;

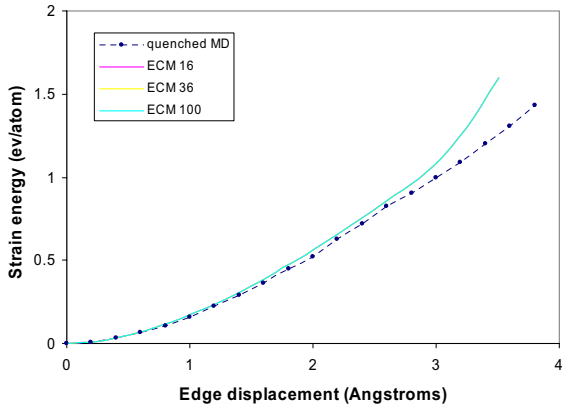

Figure 3 : Strain energy for 66-atom sheet under uniform load.

when the edge displacement becomes larger (about 3Å, approximately 25% strain), the MLPG and the quenched MD results diverge significantly, which is due to the larger cut-off zone used in the quenched MD simulation [Chung, Namburu, and Henz (2004)]. The results for 4×4, 6×6, and 10×10 nodes are nearly identical; thus demonstrating the viability of the present method.

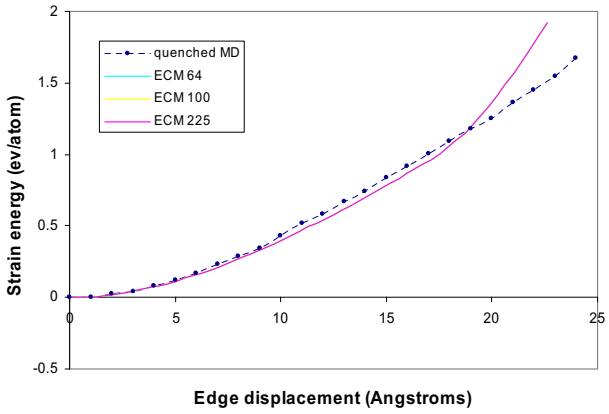

Figure 4 : Strain energy for 1952-atom sheet under uniform load.

Fig. 4 shows the strain energies for 1952-atom sheet under uniform displacement load. The same trend as in 66-atom sheet can be found: the MLPG results and the quenched MD results agree very well at small strains, and show good agreement up to approximately 25% strain. Also, the results for the different node refinements are nearly identical.

The comparison of strain energy between the MLPG method and quenched MD under the non-uniform displacement loads are shown in Fig. 5 and Fig. 6 for 66-atom and 1952-atom sheet, respectively. Same as in uniform load case, the MLPG results and the quenched MD results agree very well at small strains. Again, there are no distinguishable differences among the different node refinements.

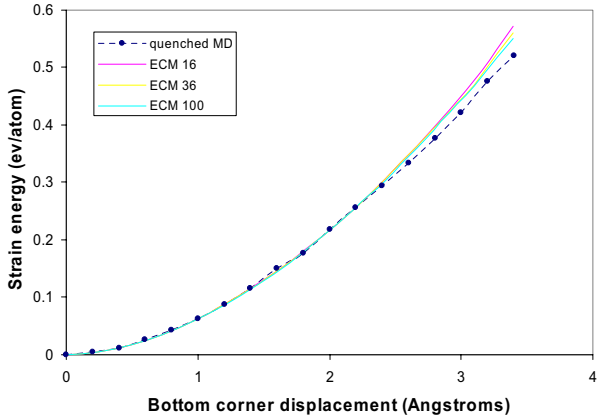

Figure 5 : Strain energy for 66-atom sheet under non-uniform load.

It should be pointed out that, compared with the method in Chung, Namburu, and Henz (2004), the method developed in this paper is computationally faster. Similar to Chung, Namburu, and Henz (2004), the numerical convergence is defined as the point where doubling the number of displacement increments changes the final energy of the system by less than 0.05%. In this method, the number of displacement increment steps needed for the convergence at 20% strain is 20, and at each increment step, the number of the Newton-Raphson iterative steps is less than 10. In Chung, Namburu, and Henz (2004), the number of displacement increment steps is 200, and at each increment step, the number of the Newton-Raphson iterative steps is less than 10.

We also consider the stability of this method. The effects of the RBF shape parameters and the radius of the trial and test function domain on the results are discussed by using the 1952-atom sheet with 10×10 nodes. The dependences of the strain energy on the RBF shape pa-

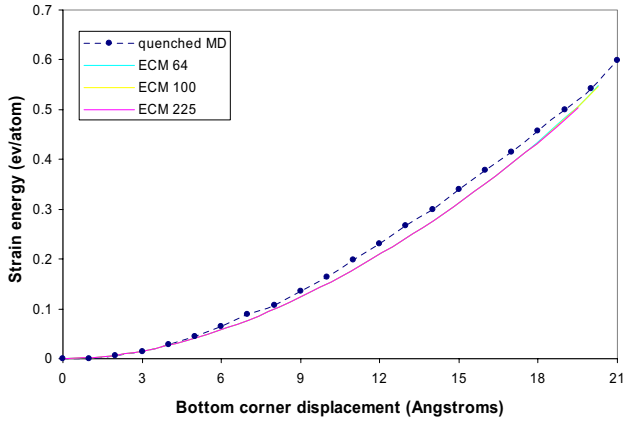

Figure 6 : Strain energy for 1952-atom sheet under non-uniform load.

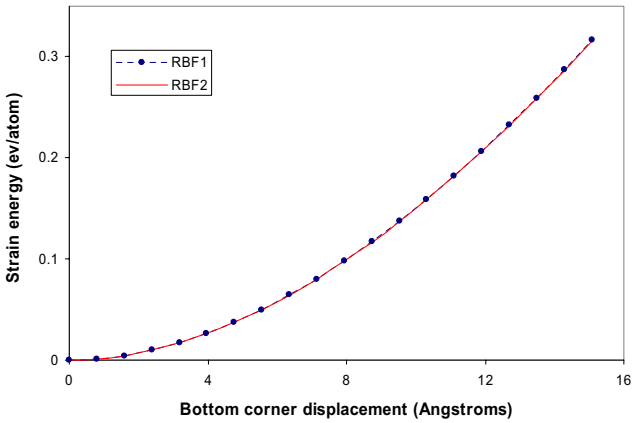

Figure 8 : Effect of the RBF shape parameters on strain energy for 1952-atom sheet under non-uniform load.

rameters are shown in Fig. 7 and Fig. 8 for uniform and non-uniform displacement loads, respectively. In these cases, the radius of the trial function domain is taken to be 3.2h, and the radius of the test domain is taken to be 0.85h. These figures indicate that different shape parameters produce the same results, which demonstrate the viability of the present MLPG method again.

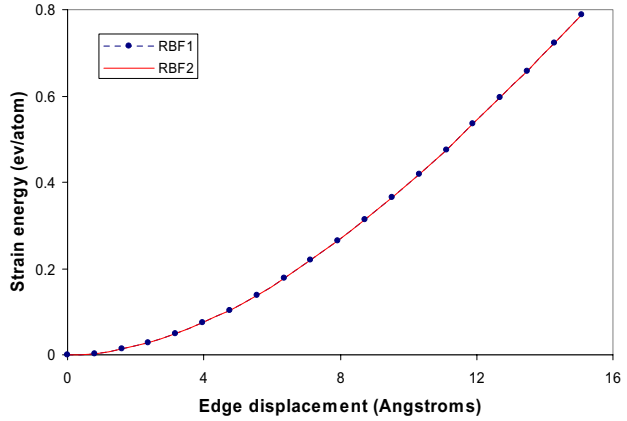

Figure 7 : Effect of the RBF shape parameters on strain energy for 1952-atom sheet under uniform load.

The effect of the radius of sub-domain (the support of the test function) is shown in Fig. 9 for non-uniform displacement load. Here, RBF2 is used. The radius of the support of the trial function is 3.2h, and the radius of the test function domain is varying from 0.55h to 0.95h. This figure shows that in the range [0.55h, 0.95h], the present method is almost independent of radius of the test function domain. The effect of the radius of the support of the trial function is shown in Fig. 10 for non-uniform displacement load. Here, RBF2 is used. The radius of the support of the test function is 0.75h, and the radius of the trial function domain is varying from 1.5h to 5.5h. Fig. 10 states that the present method is insensitive to the varying of the radius of the trial function domain from 1.5h to 5.5h. In general, the radius of the trial function domain is recommended to take from 2.0h to 3.5h, due to the computational cost. Once again, these results illustrate that the present tangent stiffness MLPG method is very stable, thus it is viable.

7.2 The ECM/molecular mechanics multiscale method

A 2D graphene sheet of one-atom thickness, with 72.8680 Å length, 37.7182 Å width, is studied in this example. There are 1060 atoms in this sheet with a 2-atom defect in the center. The molecular mechanics region is in the middle of the sheet, and two ECM regions are on the two sides of the molecular mechanics region. We study the behavior of the method for different lengths of the molecular mechanics (MM) region. Two different lengths of the MM region, 7.5380 Å and 12.5634 Å, are considered. The smaller MM region contains 124 atoms, and the larger one contains 196 atoms. The ECM region is discretized into a set of nodes. Three sets of nodes

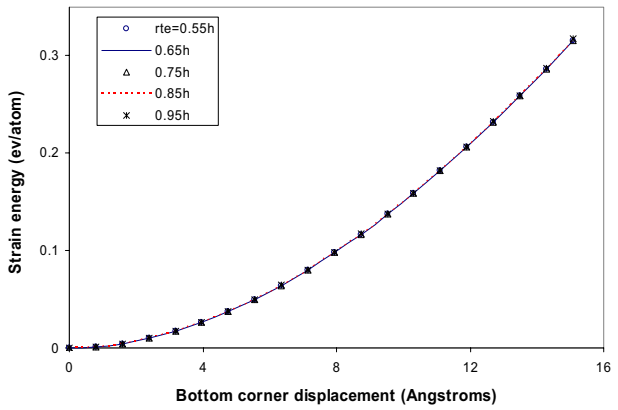

Figure 9 : Effects of the radius of the test function domain on strain energy for 1952-atom sheet under non-uniform load.

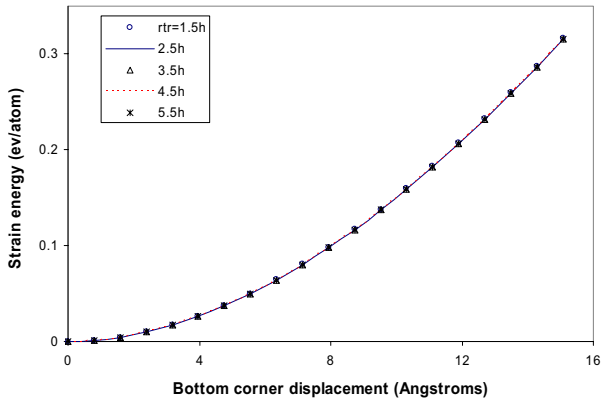

Figure 10 : Effects of the radius of the trial function domain on strain energy for 1952-atom sheet under non-uniform load.

are used in this example: 176, 84, and 40 nodes. Fig. 11 is a part of the distribution of the atoms and nodes in the reference frame for the 84-node case, where the solid circles represent the atoms, and the open triangles represent the MLPG nodes. The nodes in the region B are distributed evenly, although it is unnecessary. However, on the interface of region A and B, the nodes are taken to be the atoms, as show in Fig. 11. Actually, these nodes are only used for the interpolation, their motions are still governed by atomic balance equation (43). A uniform displacement is prescribed on the left and right edges. In the ECM region, RBF2 is used. The radius of the support of the test function is $0.83h$, and the radius of the trial function domain is $2.2h$. We also consider different radii of the support of the test and trial function domains; and the same conclusion as the full ECM/MLPG method can be reached. Hence, in this subsection, these results are not listed again.

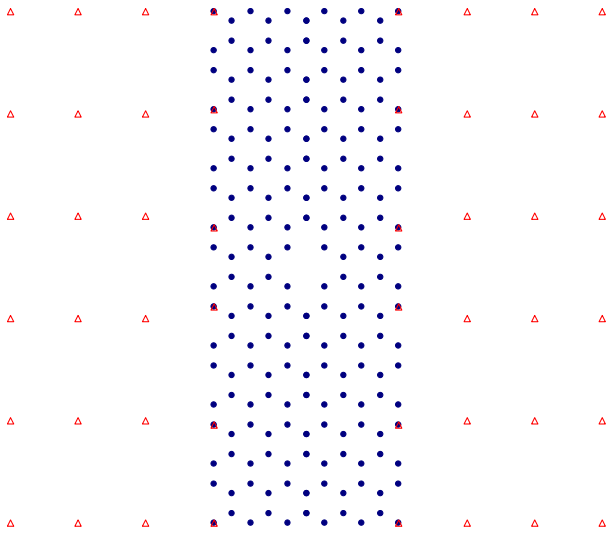

Figure 11 : The distribution of the atoms and nodes in the reference frame.

The convergence of this multiscale method is studied by using l_2 error in displacement, which is defined as

$$R_{err} = \frac{l_2(\mathbf{u} - \mathbf{u}_m)}{l_2(\mathbf{u}_m)}$$

where

$$l_2(\mathbf{u}) = \left(\sum_{I}^{N_1} \mathbf{u}_I^2 \right)$$

N_1 is the number of the atoms in the MM region (only the positions of the atoms in the MM region are includes in the error measure), $\mathbf{u}$ are the displacements of the atoms in the MM region from the multiscale method, $\mathbf{u}_m$ are the displacements of the same atoms from a full molecular mechanics calculation, which is implemented by employing the tangent stiffness formulation as discussed in Section 5. The results are shown in Fig. 12 for two different lengths of the MM region, 7.5380 Å and 12.5634 Å. In this example, the edge displacement is 4.554 Å (approximately 6% strain along the edge). The distance between the nodes along X_2-direction is normalized by the distance between the nodes along X_2-direction in 176-nodes case. It is obvious that the larger MM region gives less error in the displacements. For both sizes of the MM region, the present method is convergent. The convergence for the 12.5634 Å MM region is 3.10, and that for the 7.5380 Å MM region is 2.91.

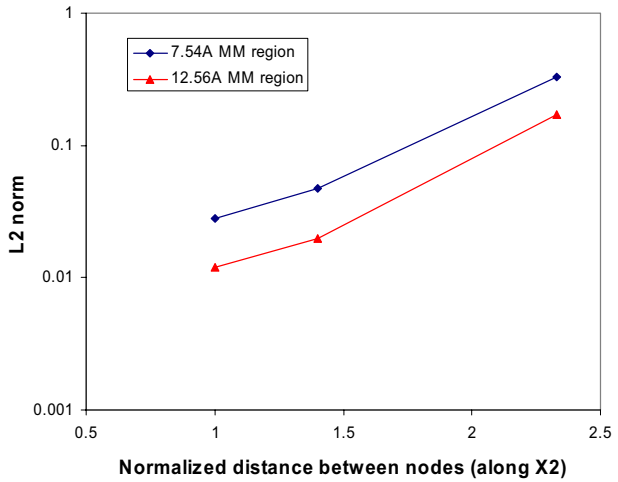

Figure 12 : Convergence of the multiscale method for different dimensions of an atom region.

Fig. 13 shows the variation of the l_2 error in displacement during the whole loading procedure. Here, the MM region is 12.5634 Å, and 176 nodes are used in the ECM region. From this figure, it is found that with the increase of the edge displacement, the l_2 error increases. This is reasonable. For large edge displacements, the deformation near the defect becomes very large. Then, the strain gradient also becomes very large in a bigger region than that for small edge displacement. In such a situation, to get more accurate results, a larger MM region is needed (the ECM region is only appropriate for the homogeneous deformation, where the strain gradient is near zero). If the molecular mechanics region is large enough, accurate enough results could be achieved. The dimension of the MM region should be adjusted according to the deformation. Hence, an adaptive scheme for this multiscale method is necessary, which will be presented in an upcoming paper.

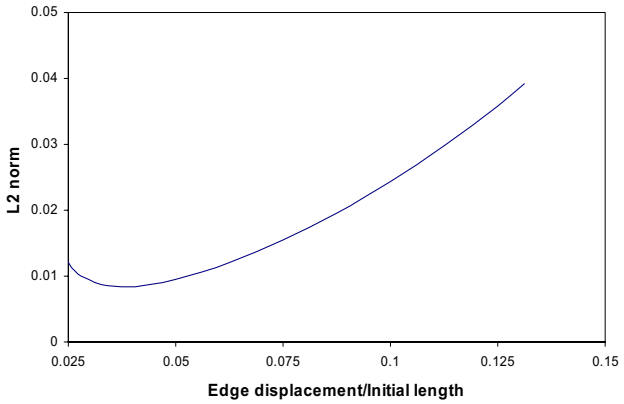

Figure 13 : The l_2 error in displacement during the whole loading procedure.

Fig. 14 shows the deformation configuration of the defected graphene sheet during the displacement procedure (only the part around the defect is plotted), which is obtained from the multiscale method. Here, the deformation is defined as ε=edge displacement/initial length. Fig. 15 is the analogous full molecular mechanics solution. These figures demonstrate that the multiscale method is quite accurate, but its computational cost is far less than that of the molecular mechanics.

In this example, for the multiscale method, the number of displacement increment steps needed for the convergence at 13% strain is 20, and at each increment step, the number of the Newton-Raphson iterative steps is less than 40; for the full molecular mechanics method, the number of displacement increment steps is 40, and at each increment step, the number of the Newton-Raphson iterative

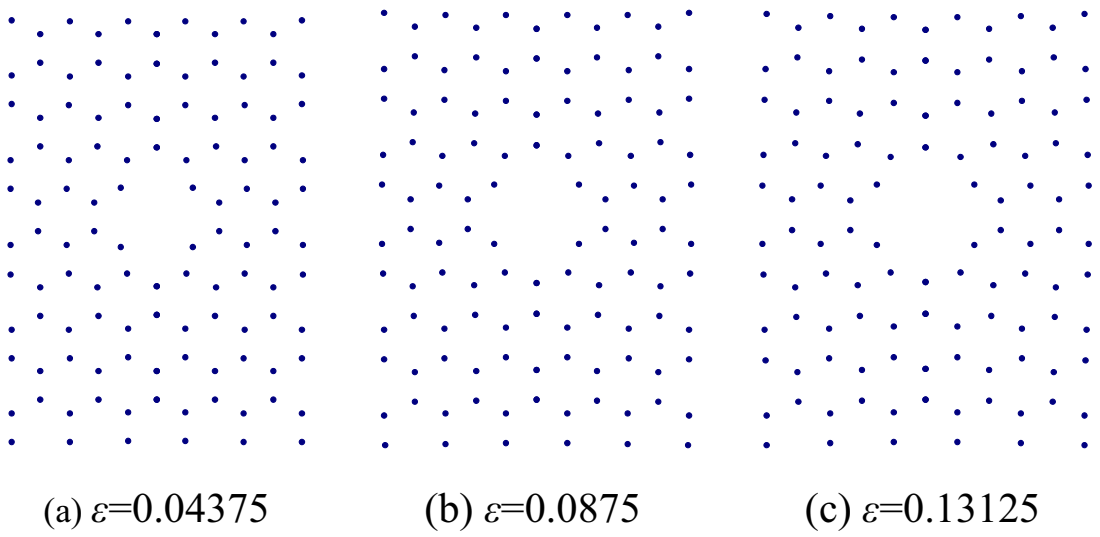

Figure 14 : Deformation configurations from the multiscale method.

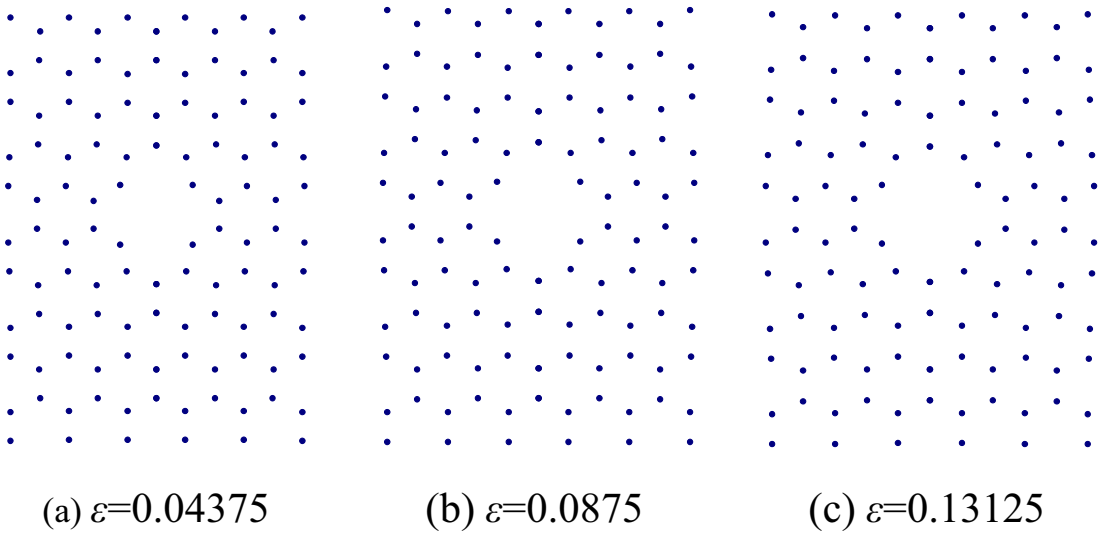

Figure 15 : Deformation configurations from the full molecular mechanics method.

steps is from 100 to 3000. This multiscale method dramatically reduces the computational time, but it still has the capability to represent the details of certain atoms.

8 Conclusion

A multiscale simulation technique, based on a combination of molecular mechanics and MLPG methods has been implemented and tested. Good agreements between this multiscale method and the full molecular mechanics method are observed in numerical examples. The linearized models are given for this multiscale method, as well as the pure molecular mechanics method, when a Newton-Raphson method is used. The tangent-stiffness MLPG method is found to be very effective and stable in multiscale simulations. This multiscale method dramatically reduces the computational cost, but it still can provide reasonable accuracy in some regions of the model.

Acknowledgement: This work was supported by the U. S. Army Research Office, and the U. S. Army Research Laboratory, under a cooperative research agreement with the University of California at Irvine. The Cognizant Program Official at the U. S. Army Research Labs is Dr. R. Namburu. Partial support for this work was also provided by the Office of Naval Research, in the program directed by Dr. Y.D.S. Rajapakse.

References

Abraham, F. F. (2000): MAADLY spanning the length scales in dynamic fracture. *CMES: Computer Modeling in Engineering & Sciences* 1 (4): 63-69.

Arroyo, M.; Belytschko, T. (2002): An atomistic based finite deformation membrance for crystalline films one atom thick. *Journal of the Mechanics and Physics of Solids* 50(9): 1941-1977.

Atluri, S. N. (1979): On rate principles for finite strain analysis of elastic and inelastic nonlinear solids. In *Recent Research on Mechanical Behavior*, 79-107, University of Tokyo Press.

Atluri, S. N. (1980): On some new general and complementary energy theorems for the rate problems in finite strain, classical elastoplasticity. *Journal of Structural Mechanics* 8(1): 61-92.

Atluri, S. N. (2004): *The meshless method (MLPG) for domain & bie discretizations*. Tech Science Press, USA.

Atluri, S. N.; Zhu, T. (1998): A new meshless local Petrov-Galerkin (MLPG) approach in computati**A**onal mechanics. *Comput. Mech*. 22: 117-127.

Atluri, S. N.; Shen, S. (2002a): *The meshless local Petrov-Galerkin (MLPG) method*. Tech. Science Press, 440 pages.

Atluri, S. N.; Shen, S. (2002b): The meshless local Petrov-Galerkin (MLPG) method: A simple & less-costly alternative to the finite element and boundary element method. *CMES: Computer Modeling in Engineering & Sciences* 3 (1): 11-52.

Atluri, S. N.; Han, Z. D.; and Shen, S. (2003): Meshless Local Patrov-Galerkin (MLPG) approaches for weakly-singular traction & displacement boundary integral equations, *CMES: Computer Modeling in Engineering & Sciences* 4 (5): 507-516.

Batra, R. C.; Ching, H. K. (2002): Analysis of elastodynamic deformations near a crack/notch tip by the meshless local Petrov-Galerkin (MLPG) method. *CMES: Computer Modeling in Engineering & Sciences* 3 (6): 717-730.

Born, M.; Huang, K. (1954): Dynamical theory of crystal lattices. Oxford: Clarendon Press.

Brenner, D. W. (1990): Empirical potential for hydrocarbons for use in simulating the chemical vapor deposition of diamond films. *Phys. Rev*. B 42(15): 9458-9471.

Cai, W.; de Koning, M.; Bulatov, V. V.; Yip, S. (2000): Minimizing boundary reflections in coupled-domain simulations. *Phys. Rev. Lett*. 85: 3213-3216.

Chung, P. W.; Namburu, R. R.; Henz, B. J. (2004): A Lattice Statics Based Tangent Stiffness Finite Element Method, *CMES: Computer Modeling in Engineering & Sciences* 5(1): 45-62.

Cousins, C. S. G. (1978): Inner elasticity. *J. Phys. C: Solid State Phys*. 11: 4867-4879.

E W.; Huang, Z. (2001): Matching conditions in atomistic-continuum modeling of materials. *Phys. Rev. Lett*. 87, art. No.-135501.

Ericksen, J. L. (1984): *Phase transformations and material instabilities in solids*. Academic Press: 61-77.

Han, Z. D.; Atluri, S. N. (2003): On Simple Formulations of Weakly-Singular Traction & Displacement BIE, and Their Solutions through Petrov-Galerkin Approaches. CMES: *Computer Modeling in Engineering & Sciences* 4 (1): 5-20.

Han. Z. D.; Atluri, S. N. (2004a): Meshless Local Petrov-Galerkin (MLPG) approaches for solving 3D Problems in elasto-statics, CMES: *Computer Modeling in Engineering & Sciences*, 6(2): 169-188.

Han. Z. D.; Atluri, S. N. (2004b): A Meshless Local Petrov-Galerkin (MLPG) Approach for 3-Dimensional Elasto-dynamics, CMC: *Computers, Materials & Continua*, 1(2): 129-140.

Hardy, R. L. (1971): Multiquadric equations of topography and other irregular surfaces. *J. Geophys. Res*. 76: 1905-1915.

Li, Q.; Shen, S.; Han, Z-D.; Atluri, S. N. (2003): Application of Meshless Local Petrov-Galerkin (MLPG) to Problems with Singularities, and Material Discontinuities, in 3-D Elasticity, *CMES: Computer Modeling in Engineering & Sciences* 4(5): 567-581.

Liu, G. R.; Gu, Y. T. (2001): A local radial point interpolation method for free vibration analysis of 2D solids. *J. Sound Vibration* 246: 29-46.

Martin, J. W. (1975): Many-body forces in solids and the Brugger elastic constants: II. Inner elastic constants. *J. Phys. C: Solid State Phys*. 8: 2858-2868.

Shen, S.; Atluri, S. N. (2004a): Multiscale simulation based on the meshless local Petrov-Galerkin (MLPG) method. *CMES: Computer Modeling in Engineering & Sciences* 5(3): 235-255.

Shen, S.; Atluri, S. N. (2004b): Computational nano-mechanics and multiscale simulation. *CMC: Computers, Materials, & Continuua* 1(1): 59-90.

Shen, S.; Atluri, S. N. (2004c): Atomic-level stress calculation and continuum-molecular system equivalence. *CMES: Computer Modeling in Engineering & Sciences* 6(1): 91-104.

Shenoy, V. B. (2003): Multiscale modeling strategies in materials science-the quasicontinuum method. *Bull. Mater. Sci*. 26(1): 53-62.

Srivastava, D.; Menon, M.; Cho, K. (2001): Computational nanotechnology with carbon nanotubes and fullerenes. *Computing in Science & Engineering* 3: 42-55.

Srivastava, D.; Atluri, S. N. (2002a): Computational Nanotechnology: A Current Perspective, *CMES: Computer Modeling in Engineering & Sciences* 3(5): 531-538.

Srivastava, D.; Atluri, S. N. (2002b): Computational Nanotechnology, Special Issue, *CMES: Computer Modeling in Engineering & Sciences* 3(5).

Tadmor, E. B.; Oritz, M.; Phillips, R. (1996): Quasicontinuum analysis of defects in solids. *Philosophical Magazine* A 73: 1529-1563.

Tadmor, E. B.; Phillips, R.; Ortiz, M. (1996): Mixed atomistic and continuum models of deformation in solids. *Langmuir* 12(19): 4529-4534.

Tang, Z.; Shen, S.; Atluri, S. N. (2003): Analysis of materials with strain gradient effects: A Meshless local Petrov-Galerkin approach, with nodal displacements only. *CMES: Computer Modeling in Engineering & Sciences* 4(1): 177-196.

Tersoff, J. (1988): Empirical interatomic potential for carbon, with applications to amorphous carbon. *Phys. Rev. Lett*. 61(25): 2879-2882.

Wagner, G. J.; Liu, W. K. (2003): Coupling of Atomistic and continuum simulations using a bridging scale decomposition. *J. Comput. Phys*. 190: 249-274.

Wendland, H. (1999): Meshless Galerkin method using radial basis functions. *Math. Comput*. 68: 1521-1531.

Zanzotto, G. (1996): The Cauchy-Born Hypothesis, nolinear elasticity and mechanical twinning in crystals. *Acta Cryst*. A52: 839-849.